PERGAMON

International Journal of Heat and Mass Transfer 45 (2002) 303–317

International Journal of HEAT and MASS TRANSFER

www.elsevier.com/locate/ijhmt

Evaporation of refrigerants in a horizontal tube: an improved flow pattern dependent heat transfer model compared to ammonia data

O. Zürcher *, D. Favrat, J.R. Thome

Department of Mechanical Engineering, Swiss Federal Institute of Technology, CH-1015 Lausanne, Switzerland

Received 18 January 2001; received in revised form 17 April 2001

Abstract

Few experimental test data are available for evaporation of ammonia inside tubes and numerous new data have been measured and presented here. An improved approach to the prediction of flow boiling heat transfer in horizontal tubes has been proposed through the study of each flow pattern separately, incorporating a new criterion defining the onset of nucleate boiling as a function of the critical convective heat transfer coefficient representative of the location where nucleate boiling might occur. A new function, based on a pseudo-Biot number delineates two different mean heat fluxes on the perimeter of the tube in stratified types of flow, one in contact with the liquid and one in contact with the vapor. Considering pure convective heat transfer, or mixed convective and nucleate heat transfer, this division allows the use of a common criterion to be applied to each flow pattern. Even if the database showed that the flow conditions in the annular liquid film were close to, or in the turbulent to laminar flow transition, and even if the major part of the experimental points where purposely obtained close to the various flow pattern transitions, the new model showed very good agreement with the experimental database of refrigerants HFC-134a and ammonia. Due to the precision of the new flow pattern map and the effectiveness of the onset on nucleate boiling criterion, this new heat transfer model accurately predicts the heat transfer conditions during evaporation. © 2001 Published by Elsevier Science Ltd.

1. Introduction

Based on our large database of two-phase flow boiling of pure ammonia in a horizontal tube, an improvement of the flow pattern oriented method of Kattan et al. [1–3] is proposed to better predict the local heat transfer coefficient of Stratified, Stratified-Wavy, Intermittent and Annular flow patterns.

Kattan [4] showed that even while different heat transfer models exist, such as the superposition, the enhancement and the asymptotic models, their range of reliable application is quite limited, essentially only to annular flows (even if those methods do not know when this regime exists). Compared to a complete database covering different flow patterns, they thus established that only flow map based heat transfer relations should today be seriously considered. Even if the method proposed by Kattan et al. [1–3] was a significant improvement compared to those prior methods, they did not have experimental data in the Stratified flow region, nor with fluids other than the HFC class of refrigerants and neither for mass velocities less than 100 kg/(m^2 s). Thus, some particular flow regions still require further analysis.

As a first attempt, Zürcher et al. [5] proposed several empirical modifications of the original flow pattern map of Kattan et al. [1], i.e., to the Stratified-Wavy to Annular and the Stratified to Stratified-Wavy transition boundaries, to better predict the local heat transfer coefficient of ammonia at low mass velocities. Based on even more recent, extensive tests covering different heat flux ranges and numerous mass velocities for ammonia, some improvements to the original method of Kattan

* Corresponding author.

E-mail addresses: olivier.zuercher@epfl.ch (O. Zürcher), daniel.favrat@epfl.ch (D. Favrat), john.thome@epfl.ch (J.R. Thome).

0017-9310/02/$ - see front matter © 2001 Published by Elsevier Science Ltd.
PII: S0017-9310(01)00145-4

Nomenclature

A	cross-sectional area (m^2)
Bi	Biot heat transfer number (dimensionless)
C	distribution factor (dimensionless)
c_0	distribution factor multiplier (dimensionless)
D	diameter (m)
D_h	hydraulic diameter (m)
d	vapor core diameter (m)
F_1	Biot function (dimensionless)
Fr	Froude number (dimensionless)
G	mass velocity ($kg/(m^2\ s)$)
g	acceleration of gravity (m/s^2)
h	enthalpy per unit of mass (J/kg)
Δh_{evap}	latent heat (J/kg)
h	heat transfer coefficient ($W/(m^2\ K)$)
$\underline{M}$	molecular weight (kg/kmol)
$\dot{M}$	flowrate (kg/s)
P	pressure (Pa)
Pr	Prandtl number (dimensionless)
p	non-dimensional function (dimensionless)
$\dot{q}$	heat flux (W/m^2)
$\dot{Q}$	heat duty (W)
Re	Reynolds number (dimensionless)
r	radius (m)
S	contact perimeter (m)
T	temperature (K)
u	velocity (m/s)
V	drift velocity (m/s)
x	vapor quality (dimensionless)
X_{tt}	Martinelli parameter (dimensionless)

Greek symbols

α	void fraction (dimensionless)
δ	liquid layer thickness (m)
ε_i	relative error (dimensionless)
ζ	abscissa along the tube (m)
θ_{dry}	dry angle (rad)
θ_{wet}	wetted angle (rad)
λ	thermal conductivity (W/(m K))
μ	dynamic viscosity (Pa s)
ξ	Stratified-Wavy angle (rad)
ρ	density (kg/m^3)
σ	surface tension (N/m)
σ	standard deviation (dimensionless)
φ	Stratified-Wavy opening angle (rad)
ψ	Stratified-Wavy wetting angle (rad)

Subscripts

A	annular
cb	convective boiling
crit	critical
I	intermittent
i	interface
in	inlet
L	liquid
nb	nucleate boiling
ONB	onset on nucleate boiling
out	outlet
sat	saturation
Strat	Stratified
Wavy	Stratified-Wavy
tp	two-phase
V	vapor
vap	all vapor
w	wall
wat	water
wet	wetted
$\tilde{(\ )}$	non-dimensional value of a parameter

et al. [3] for prediction of the local heat transfer coefficient were found to be necessary to better model the onset of dryout phenomenon, the effect of heat flux and the non-uniformity of the heat flux around the tube for stratified types of flow.

2. Test conditions

The experimental test section is composed of two concentric tubes, with evaporation of the refrigerant inside the inner tube and counter-current water heating in the annulus. A new database of the local heat transfer coefficients and flow pattern visualization for ammonia have been collected and used to develop a new and more general heat transfer model.

In these tests, ammonia was evaporated at 4°C in a 439 grade stainless steel tube of 15.86 mm outside diameter. The global conditions were an internal tube diameter of 14.00 mm, a heat flux range of 5–70 kW/m^2 and 11 mass velocities of $G = 10$, 20, 30, 40, 45, 50, 55, 60, 80, 120, 140 $kg/(m^2\ s)$ corresponding to Stratified, Stratified-Wavy, Intermittent and Annular flow patterns. Complementary tests, varying the mass velocity at constant vapor qualities ($x = 20\%$, 50%, 80%), were then made to better characterize the transition boundaries between flow patterns and to observe the variation in heat transfer coefficients across these boundaries. The flow patterns are observed and videotaped through a tubular glass section at the exit of the 3.1 (m) long test tube.

The flow patterns observed were classified as follows: Stratified (S), Stratified-Wavy (SW), Intermittent (I) and Annular (A), and transitions between these regimes. For instance, the transition between Intermittent and Annular flow regimes was designated as I/A. Complementary

information about the flow regimes and the development of a diabatic two-phase flow pattern map are given in [6].

3. Heat transfer measurements

The original version of the test rig used for the HFCs tests has already been described in detail by Kattan et al. [2] while the description of the modifications to the test loop for the ammonia tests have been described in [5]. Hence, only a brief description is presented below. Fig. 1 shows a simplified diagram of the test section.

The good heat transfer properties of ammonia compared to HFCs and the water-side made it inaccurate to rely on the Wilson plot approach for these tests and hence the definition of the heat transfer coefficient itself was applied ($h = \dot{q}_{in}/(T_w - T_{sat})$). Thus, external wall temperatures were measured by thermocouples and corrected for radial conduction through the heat transfer tube to obtain the internal wall temperature. The saturation temperatures of the refrigerant, T_{sat}, were obtained from the absolute and differential pressure measurements applied to the measurement location. Specifically, two fully independent measurement locations were installed in the tube at 2000 and 2500 mm from the entrance of the 3010 mm long tube. Four 0.25 mm thermocouples circumferentially distributed were embedded in the wall at each location (at 0°, 60°, 120° and 180° from the top). A 0.3 mm groove was made for each thermocouple to be inserted whose sides were then pinged to hold the thermocouple in place. The mean of these four internal wall temperatures were used for T_w.

As shown in Fig. 2 an augmentation wire was twisted on the outside of the test tube to enhance mixing of the water and to reduce the temperature difference between the external tube wall and the bulk of the water flow, which was key to the very accurate measurements obtained with ammonia. A picture of the twisted wire around the heated tube with the embedded wall thermocouples is presented in Fig. 2.

The temperature of the water in counter-current flow is measured at four different locations along the tube. Each location includes four thermocouples (calibrated to an accuracy of ±0.02°C). These measurements are

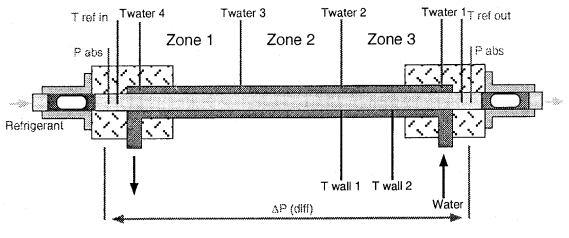

Fig. 1. Diagram of the test section.

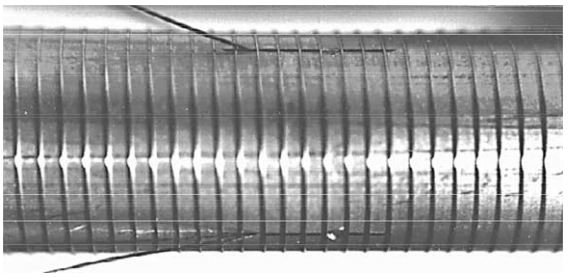

Fig. 2. Picture of the twisted wire of 0.2 mm diameter around the heated tube and wall thermocouples of 0.25 mm.

used to calculate the vapor quality of the refrigerant at these four locations along the tube and the heat flux.

The local heat flux $\dot{q}_{in}$ along the flow channel was obtained as follows. Since the variation of density of water between 0°C and 20°C is only about 0.075% and therefore the variation of kinetic energy along the tube can be neglected, the heat duty for the water side can be deduced to be

$$\dot{Q}^- = [h_2 - h_1]\dot{M}_{wat}, \tag{1}$$

where h is the enthalpy at locations 1 and 2 and $\dot{M}_{wat}$ is the mass flowrate of water (measured with a Coriolis meter to ±0.5% of flow). Based on the mean water temperatures at four locations along the tube (obtained from the four thermocouples in the water at each location), a Lagrange polynomial of third-order $P_3(\zeta)$ expressing the enthalpy change of the water along the tube axial position ζ is obtained. The internal heat flux $\dot{q}_{in}$ on the refrigerant is then obtained by the derivative of the Lagrange polynomial

$$\dot{q}^+_{in}(\zeta) = \dot{q}^-_{out}(\zeta)\frac{D_{out}}{D_{in}} = \frac{\dot{M}_{wat}}{\pi D_{in}}\frac{dP_3(\zeta)}{d\zeta}. \tag{2}$$

For all experimental tests, the Lagrange polynomial and its derivative are calculated, and then used to calculate the vapor quality and heat flux at the two measurement locations along the tested tube. As a double check of this approach, the internal heat flux calculated with the Lagrange polynomial was compared to the mean heat flux calculated with the heat duty divided by the heated surface of a zone and showed comparable values. Based on an analysis of propagation of errors, the relative error of the local heat transfer coefficient is about 10%, while the error of the internal heat flux is less than 3%. For complementary information, please refer to [7].

4. Experimental results

Some of the experimental tests described here were already published in [5] and compared to the heat transfer model of Kattan et al. [3] as well as their heat

transfer model with empirical modifications to their flow pattern map proposed by Zürcher et al. [5]. New experimental data at a given mass velocity over a range of vapor quality are presented here for $G = 10$ and 30 kg/(m^2 s), and the results for numerous tests at constant vapor quality ($x = 20\%$, 50%, 80%) with variation of the mass velocity. In addition, an enlarged database for heat flux in Annular flow (concerning $G = 80$, 120, 140 kg/(m^2 s)) have also been measured for extension of the heat transfer model.

4.1. Comment about the figures

The experimental results are plotted as squares, and the predicted heat transfer coefficients, calculated with the experimental conditions of each individual data point, are plotted as a line. Since hot water is used as the heating source, pre-established heat fluxes cannot be run and data for a range of heat flux are shown at the mean of the group. Most of the heat fluxes are within ±15% of the mean value cited in each graph. Due to this, the predicted curves are not smooth since the specific test conditions at each point are used to produce it. Even if this method is not rigorous (there is no physical meaning of the *line* between two calculated points), it helps to better visualize the relationship and improves comprehension. The experimental results (with predictions) are shown first and then the new improvements to the heat transfer model are described.

4.2. The Stratified heat transfer region

Fig. 3 shows new local heat transfer results and predictions for $G = 10$ kg/(m^2 s) at mean heat fluxes of 7.13 and 8.74 kW/m^2. Transition from Stratified flow to Stratified-Wavy flow occurs at $x = 68\%$. The limited number of experimental points is due to the difficulty and time required to obtain stable flow conditions at these extremely low mass velocities. Consider for example that the time needed for a refrigerant molecule to circulate through the entire loop was about 55 min, mainly due to the capacity of the shell-and-tube condenser. Thus, a stabilization time of about one hour between two experimental points was needed to insure steady flow conditions.

For these two tests at $G = 10$ kg/(m^2 s), the heat flux affects the experimental local heat transfer coefficient. In this domain the heat transfer coefficient depends on nucleation and convection, the latter being quite small due to the very low velocity of the flow.

4.3. The Stratified to Stratified-Wavy heat transfer region

Fig. 4 shows experimental and predicted heat transfer coefficients in a region with some pure Stratified, but mainly with Stratified-Wavy flow patterns (experimental results already published by Zürcher et al. [5]). A significant effect of heat flux on the heat transfer coefficient is obtained. Convective heat transfer plays only a marginal influence, while primarily the heat transfer is driven by nucleate boiling at this low flowrate.

4.4. The Stratified-Wavy heat transfer region

Fig. 5 shows new local heat transfer coefficient results obtained at $G = 30$ kg/(m^2 s). Some pure Stratified-Wavy results with a short occurrence of Stratified flow were observed. It can be noted that the global magnitude of the local heat transfer coefficients has been correctly predicted. Nevertheless, the increasing slope of the experimental results has not been respected by the model, but this phenomena is not evident in Figs. 4 and 6 and there is no clear explanation for this rising slope in Fig. 5.

Fig. 6 shows the local heat transfer results obtained at $G = 45$ kg/(m^2 s) (experimental results already published by Zürcher et al. [5]) where the flow pattern is primarily Stratified-Wavy. The local heat transfer coefficient is almost constant in the vapor quality range from 10% to 85%. The fluctuations in the predicted curve are the result of the experimental heat flux of the individual points that are just above or below the onset of nucleate boiling.

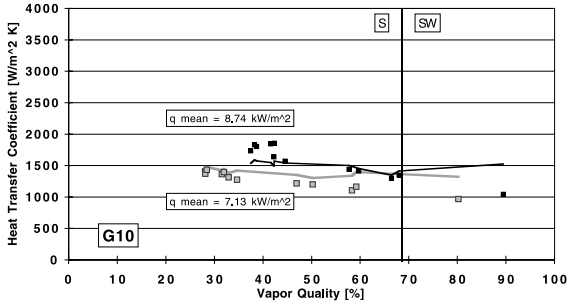

Fig. 3. Comparison of experimental results (squares) to the new model for ammonia at $G = 10$ kg/(m^2 s).

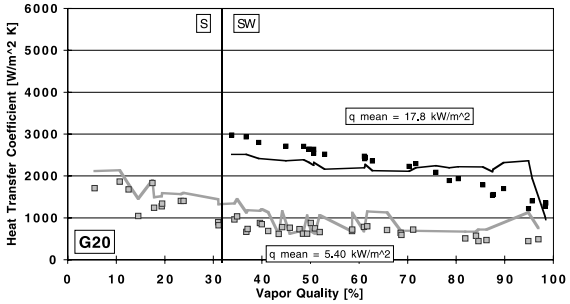

Fig. 4. Comparison of experimental results (squares) to the new model for ammonia at $G = 20$ kg/(m^2 s).

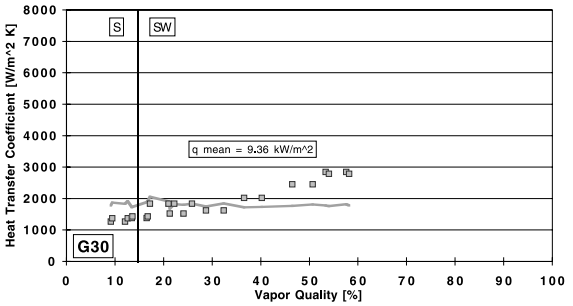

Fig. 5. Comparison of experimental results (squares) to the new model for ammonia at $G = 30$ kg/(m^2 s).

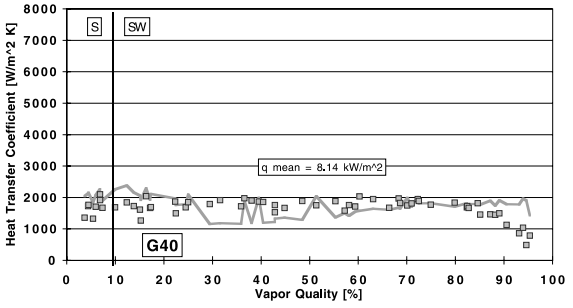

Fig. 6. Comparison of experimental results (squares) to the new model for ammonia at $G = 40$ kg/(m^2 s).

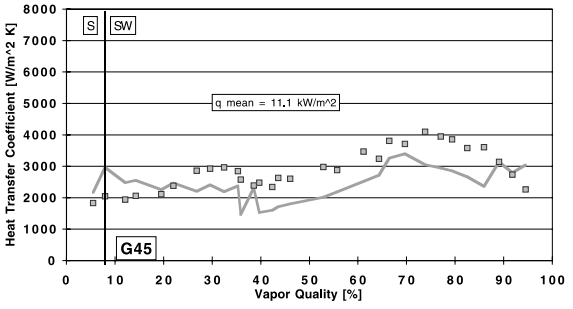

Fig. 7. Comparison of experimental results (squares) to the new model for ammonia at $G = 45$ kg/(m^2 s).

Fig. 7 shows the local heat transfer results at $G = 45$ kg/(m^2 s) (experimental results already published by Zürcher et al. [5]). The purpose of these particular tests was to better define the transitional zone between Stratified-Wavy and Annular flow patterns. Note that the variation from $G = 40$ to $G = 10$ kg/(m^2 s) means a variation of flowrate of only about 2 kg/h.

The general tendency of a rise in the local heat transfer curve towards the Annular heat transfer characteristic is particularly evident on this graph. Even so, the flow pattern is still Stratified-Wavy. In the sight glass observations, it was noticed that while the flow was mostly Stratified-Wavy, when the top of the tube was occasionally wetted with a fluid its motion was much slower along the tube compared to the bottom of the tube.

4.5. The Stratified-Wavy to Annular heat transfer region

Even if the Annular flow pattern region is still not reached at 45 kg/(m^2 s), the next small step increase in the mass velocity from 45 to 50 kg/(m^2 s) shows a strong tendency towards a heat transfer shape typical of Annular flow. Fig. 8 shows two different mean heat fluxes (experimental results already published by Zürcher et al. [5]). It can be shown that there is an important influence of heat flux on the local heat transfer coefficient, and the typical peak is clearly appearing at a vapor quality of 75%. Note that at this value, the experimental heat transfer coefficient is scattered, which demonstrates the sensitivity of the wetted angle in the region close to the Annular flow pattern.

Fig. 9 represents the experimental points at $G = 60$ kg/(m^2 s) (experimental results already published by Zürcher et al. [5]), which basically confirm the trend previously mentioned to delineate the secondary peak occurring at $x = 22\%$ and for the onset of Annular flow. The sharp fall in the heat transfer coefficient at the onset

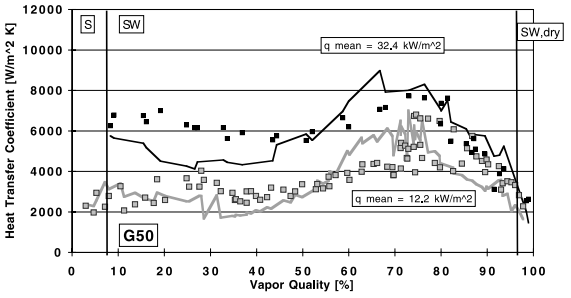

Fig. 8. Comparison of experimental results (squares) to the new model for ammonia at $G = 50$ kg/(m^2 s).

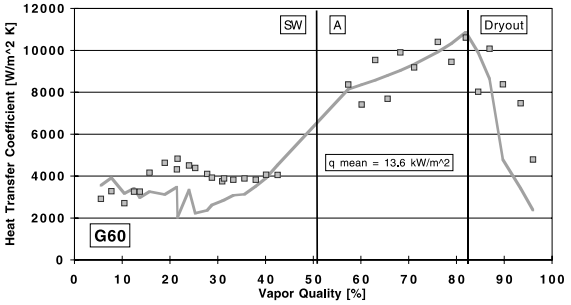

Fig. 9. Comparison of experimental results (squares) to the new model for ammonia at $G = 60$ kg/(m^2 s).

of dryout at the top of the tube at $x = 82\%$ is also clearly evident.

4.6. The Annular (and Dryout) heat transfer region

A wide number of experimental data have been collected at $G = 80$ kg/(m^2 s). Due to the proposed modification of the Stratified-Wavy to Annular transition of Kattan et al. [1], the effect of heat flux on the local heat transfer coefficient and on the onset of Dryout prediction at high vapor quality has been extensively investigated.

Figs. 10 and 11 show complete evaporation at very different heat flux ranges (experimental results at heat flux ranges of 13.0, 17.8 and 32.5 kW/m^2 were already published by Zürcher et al. [5] while the other are new data). Based on the experimental measurements, no major enhancement of the heat transfer coefficient due to heat flux has been observed in Annular flow.

As shown in Fig. 10, the experimental peaks occur nearly at the same vapor quality, which means that no major influence on the onset of dryout due to heat flux exists at least below some threshold value. On the other hand, Fig. 11 clearly shows an influence of heat flux as the peak has been shifted to lower vapor quality values.

Based on the experimental points in Figs. 10 and 11, the location of the onset of dryout location is seen to be the same until a given heat flux is reached. Furthermore, the peak when $\dot{q} < 45$ kW/m^2 is characterized by a liquid Reynolds value of $Re_{DL} \approx 650$. Due to this, the Stratified-Wavy to Annular flow transition has been set to follow this transitional Reynolds number as long as the heat flux range was smaller than a given value based on experimental results (refer to [6]). Globally, the heat flux has acted on the ammonia liquid film for heat fluxes higher than 45 kW/m^2.

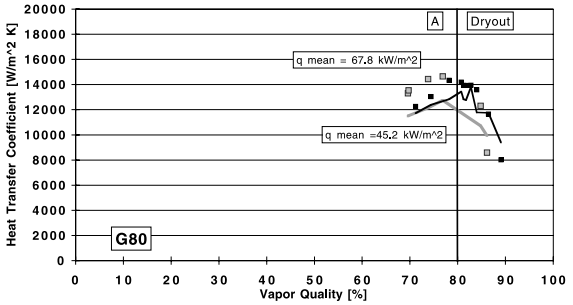

Fig. 11. Comparison of experimental results (squares) to the new model for ammonia at $G = 80$ kg/(m^2 s) at moderate to high heat fluxes.

Fig. 12 shows the experimental points at $G = 120$ kg/(m^2 s) at three different heat fluxes spanning to flow regimes. As observed for all the Annular flow data in the present database, there is no major effect of heat flux on the experimental heat transfer coefficient. In contrast, in the Stratified-Wavy region the effect of heat flux is significant.

Figure 13 shows the experimental points at $G = 140$ kg/(m^2 s) at low and high heat fluxes. The comments

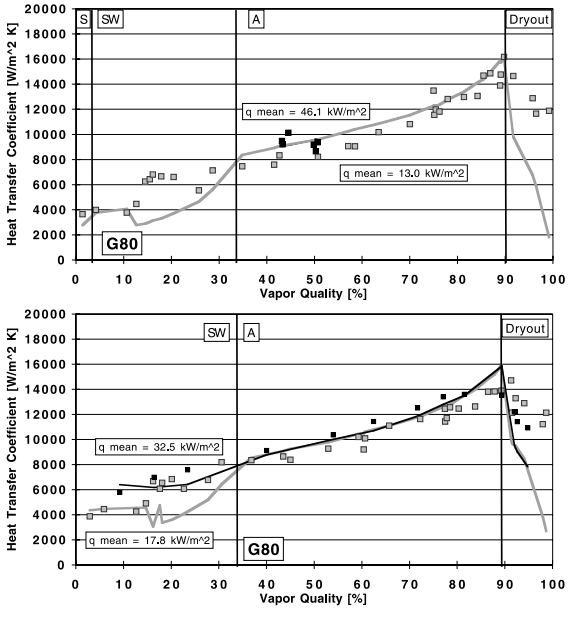

Fig. 10. Comparison of experimental results (squares) to the new model for ammonia at $G = 80$ kg/(m^2 s). Effect of heat flux on Annular heat transfer.

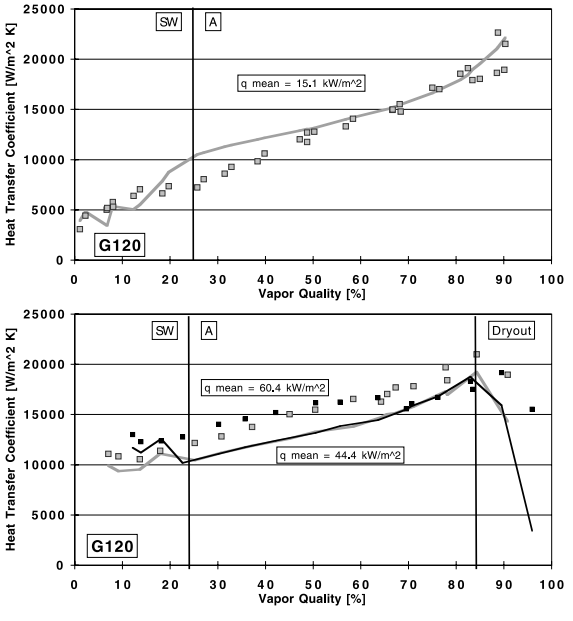

Fig. 12. Comparison of experimental results (squares) to the new model for ammonia at $G = 120$ kg/(m^2 s) at low heat flux.

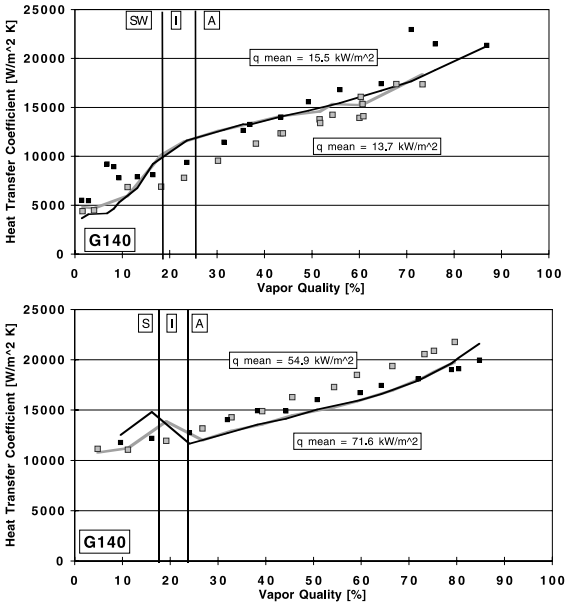

Fig. 13. Comparison of experimental results (squares) to the new model for ammonia at $G = 140$ kg/(m^2 s) at different heat fluxes.

about the experimental points are almost identical to those at $G = 120$ kg/(m^2 s), where the heat flux only influences the heat transfer coefficient in the Stratified-Wavy region.

4.7. Heat transfer at constant vapor quality

Running experimental tests at constant mass velocity with a variation in vapor quality is typical of most boiling tests. However, this type of test mode is not a suitable for defining the locations of the flow regime transition boundaries. Referring to a given flow map given in G vs. x, the experimental tests at constant mass velocity follow a horizontal line. At low mass velocities, two transition boundaries may be crossed during evaporation, these are the Stratified to Stratified-Wavy and the Stratified-Wavy to Annular transitions. As these transition boundaries are nearly horizontal themselves over a broad range of vapor quality, and due to the fact that a transition *zone* is not a transition *line*, it seems evident that the real location of the transition might not be properly located with tests at constant mass velocity with varying vapor quality. Thus, although this type of test is very time consuming to perform tests at constant vapor quality with variation of the mass velocity were made for a large number of mass velocities. In respect to the condition of *constant* vapor quality, only measurement points located between $19.00 < x < 20.99\%$ where included for the tests at $x = 20\%$. The same procedure has been adopted for the two other constant vapor qualities.

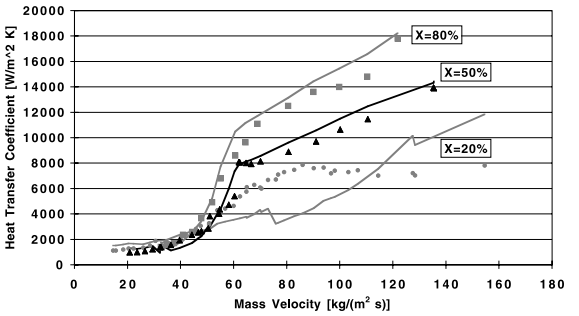

Fig. 14. Comparison of experimental results (squares) to the new model for ammonia at three constant vapor qualities 20%, 50%, 80% and varying the mass velocity (mean heat flux of 14.0 kW/m^2).

Three fixed vapor qualities were tested and these new results are shown in Fig. 14. The first at $x = 20\%$ (mean heat flux of $\dot{q} = 14.0$ kW/m^2) was used to define the validity of the Intermittent to Annular transition beginning at the Stratified-Wavy to Annular transition boundary. The second at $x = 50\%$ (mean heat flux of $\dot{q} = 13.5$ kW/m^2) was used to define the location of the lowest mass velocity of the Stratified-Wavy to Annular transition. It has been established that the transition occurs for ammonia at $G = 60$ kg/(m^2 s) for the above mentioned vapor quality. This transition can be shown in terms of heat transfer by a step change increase of the heat transfer coefficient in Fig. 14. The third test was run at $x = 80\%$ (mean heat flux of $\dot{q} = 14.8$kW/m^2) to define the sensitivity of the wetted angle in the Stratified-Wavy zone, and naturally to define the transition to Annular flow. In this case, only the last point has been identified to be Annular.

All three constant vapor qualities tested are shown in Fig. 14. At low mass velocity (when the flow pattern is Stratified and Stratified-Wavy), it is seen that the three curves are nearly identical. This means that the heat transfer coefficient is a constant value (naturally when the very low and very high vapor qualities are avoided), which is confirmed by the constant tendency of the heat transfer coefficient in Figs. 3, 4 and 6. Then, as the mass velocity increases, the slope of the heat transfer curve at $x = 80\%$ is higher than the one at $x = 50\%$ which is also higher than the last at $x = 20\%$, which is typical to higher mass velocities as shown in Figs. 9–13. The new model in fact predicts the trends at $x = 50\%$ and $x = 80\%$ but it is not able to capture that at $x = 20\%$.

5. Heat transfer flow models

5.1. Geometrical representation of the flow patterns

The Stratified flow pattern is characterized by the separation of the liquid and vapor phases by a smooth

horizontal interface. This flow pattern occurs at very low mass velocities when the Kelvin–Helmholtz instability criterion is counter-balanced by the viscous forces. The geometrical equations for the respective cross-sectional areas and contact perimeters of the two phases in the Stratified flow configuration are given in [6]. For this flow pattern, the void fraction α is a direct function of the wetted angle θ_{wet}

$$\alpha = \frac{2\pi - \theta_{wet} + \sin\theta_{wet}}{2\pi}. \tag{3}$$

From a geometrical point of view and assuming no liquid entrainment in the vapor core, the Annular flow configuration is fully determined with void fraction as long as the Annular flow pattern is characterized by an all wetted perimeter with a circular vapor core of diameter d, as shown in Fig. 15. The vapor core may either be centered or eccentric with respect to the central axis of the tube. The particular case where no liquid droplets are entrained in the vapor core is called the ideal Annular configuration, where

$$\alpha = \left(\frac{d}{D}\right)^2. \tag{4}$$

As originally proposed by Kattan et al. [3], the geometrical representation of Intermittent flow pattern is, for simplicity, assumed to be that of the Annular model using the same heat transfer model as for Annular flow, also based on the mean liquid layer δ. Because of the lower void fraction values, the liquid layer should no more be considered as very small compared to the tube diameter. Nevertheless, Kattan [4] obtained very accurate results in this unsteady flow region (Intermittent flow), and the same assumption is made here for the new model.

The Stratified-Wavy flow pattern is more difficult to represent geometrically since the wetted angle is an independent variable. As shown in Fig. 16, the liquid cross-sectional surface can be modelled by the intersection of the inner tube wall and a second circle centered at $0'$ with a radius of R_0. The parameterization of the circle is set as a function of two angles, called here the *half wetting angle* ψ and the *moon angle* φ. The difference between these two angles is called the *Stratified-Wavy angle* ξ. The corresponding void fraction is

$$\alpha = 1 - \frac{1}{\pi}\left[\left(\psi - \frac{1}{2}\sin(2\psi)\right) - \frac{\sin^2\psi}{\sin^2\xi}\left(\xi - \frac{1}{2}\sin(2\xi)\right)\right]. \tag{5}$$

The wetting angle is a key parameter in the present model because the two-phase flow mean heat transfer coefficient around the periphery is a direct proration of the liquid and vapor heat transfer coefficients for the wet and dry perimeters, as originally proposed by Kattan et al. [3]

$$h_{tp} = \frac{\theta_{dry}h_V + (2\pi - \theta_{dry})h_{wet}}{2\pi}. \tag{6}$$

The convective heat transfer coefficient of the vapor h_V is based on the Dittus–Boelter correlation [16] for tube flow, as follows:

$$h_{cb,V} = 0.023\, Re_{DV}^{0.8}\, Pr_V^{0.4}\, \frac{\lambda_V}{D_{h,V}}, \tag{7}$$

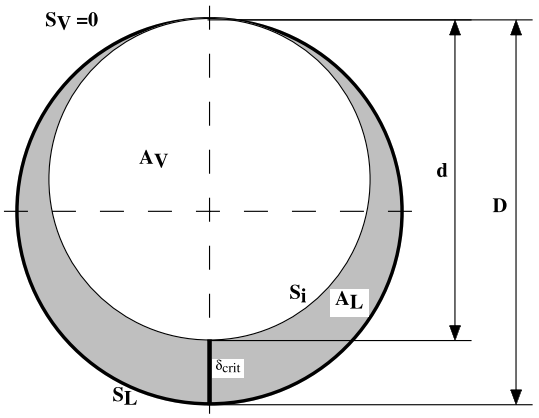

Fig. 15. Cross-section of ideal Annular configuration.

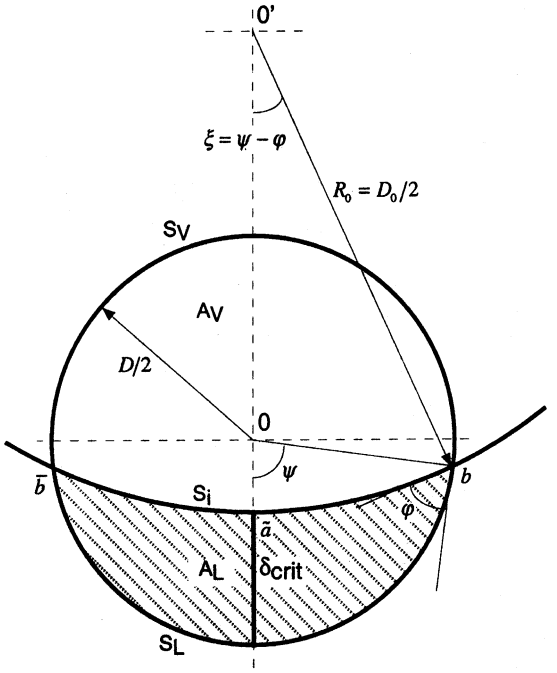

Fig. 16. Modeling of the Stratified-Wavy flow pattern based on the intersection of two circles.

where $D_{h,V}$ is the hydraulic diameter for the perimeter in contact with the vapor, assuming the interface to be a smooth motionless wall. As the void fraction tends rapidly to one during evaporation, the hydraulic diameter is very close to the value of the tube diameter.

For the liquid, the heat transfer coefficient h_{wet} is either purely convective or a combination of nucleate and convective contributions. The distinction is obtained by the comparison of the heat flux to that for the onset of nucleate boiling (ONB), which is detailed in the next section. Thus, for a heat flux over the ONB, the liquid heat transfer coefficient is calculated with the same asymptotic model used by Kattan et al. [3], defined as

$$h_{wet} = \left[(h_{cb,L})^3 + (h_{nb})^3 \right]^{1/3}, \tag{8}$$

where h_{nb} is the nucleate pool boiling contribution calculated with the relation of Cooper [8], which is

$$h_{nb} = 55 \left(\frac{P}{P_{crit}} \right)^{0.12} \left[-\log \left(\frac{P}{P_{crit}} \right) \right]^{-0.55} \underline{M}^{-0.5} \dot{q}^{0.67}. \tag{9}$$

This nucleate pool boiling correlation is based on over 6000 experimental points related to over 100 publications.

For the case where the heat flux is smaller than the ONB value, the nucleate boiling contribution h_{nb} is set to zero and thus, from Eq. (8), the liquid heat transfer coefficient is purely convective ($h_{wet} = h_{cb,L}$), and is calculated with the forced convection relation applied to this liquid layer:

$$h_{cb,L} = 0.01361 \, Re_{\delta}^{0.6965} \, Pr_L^{0.4} \, \frac{\lambda_L}{\delta}. \tag{10}$$

Note that the constants in Eq. (10) are based on experimental points (refer to Fig. 17).

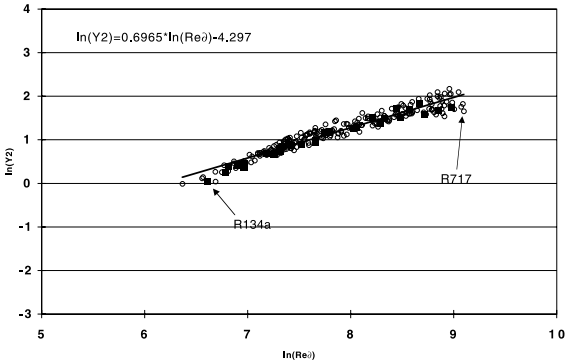

Fig. 17. Determination of the leading constant C and the Reynolds number exponent m assuming pure convective heat transfer, based on ammonia measurements in Annular flow. Note that data for Reynolds numbers $\geqslant 650$ are well represented with a forced convection turbulent heat transfer model.

5.2. The onset of nucleate boiling criterion (ONB)

Based on the experimental heat transfer results, Zürcher et al. [9] proposed a new criterion to differentiate pure convective evaporation to mixed nucleate and convective flow boiling compared to that of Steiner and Taborek [10] for evaporation in vertical tubes. The heat transfer model is purely convective for heat flux values lower than

$$\dot{q}_{ONB,x} = \frac{2\sigma T_{sat} h_{cb,crit}}{r_{crit} \rho_V \Delta h_{evap}}, \tag{11}$$

where $h_{cb,crit}$ is the convective heat transfer coefficient occurring during evaporation at the current vapor quality, and at the most advantageous location in the liquid cross-section:

$$h_{cb,crit} = C \, Re_{\delta}^{m} \, Pr_L^{0.4} \frac{\lambda_L}{\delta_{crit}}. \tag{12}$$

As convective boiling is inversely proportional to the liquid thickness, the onset of nucleate pool boiling should occur at the location where the liquid thickness is the largest (δ_{crit}).

The values of the two constants $C = 0.01361$ and $m = 0.6965$ are based on experimental results of purely convective heat transfer in Annular flow for $Re_L > 650$ (see Fig. 17). It seems unrealistic to allow the turbulent to laminar transition to occur to values as low as proposed above. But the analysis of the convective heat transfer model showed that the flow regime is still turbulent for this Reynolds number. Normally the flow regime should become laminar at the transitional value of $Re \approx 1250$ for liquid Annular flow modelled as a liquid layer. If this were the case, it would not be feasible to model both laminar and turbulent heat transfer coefficients through a unique equation over the Reynolds number range in Fig. 17. Thus, since a single equation fits the data, it can be concluded that the flow remains turbulent down to the proposed Reynolds number of $Re_D \approx 650$.

The film Reynolds number referred to a liquid layer is

$$Re_{\delta} = \frac{4\rho_L u_L \delta}{\mu_L}. \tag{13}$$

Based on the geometrical representations of the flow patterns, the critical layer thickness applied to Stratified flow is

$$\delta_{crit,Strat} = \frac{D}{2} \left(1 - \cos \frac{\theta_{wet}}{2} \right). \tag{14}$$

For Stratified-Wavy flow pattern, the critical layer thickness is

$$\delta_{crit,Wavy} = \frac{D}{2} \left(1 - \frac{\cos\psi + \cos\varphi}{1 + \cos(\psi - \varphi)} \right). \tag{15}$$

The Annular flow liquid thickness varies between the mean film thickness and twice its value, which is due to the horizontal configuration (Fig. 15). Here twice the mean liquid layer is chosen as it corresponds to the thickest possible liquid layer in Annular horizontal flow (Eq. (16)). It occurs along the Stratified-Wavy to Annular flow transition and gives the smallest onset value $\dot{q}_{\mathrm{ONB,x}}$. Even so, the calculated threshold for ONB was higher than most experimental heat fluxes tested here

$$\delta_{\mathrm{crit,A}} = D - d = 2\frac{D}{2}\left(1 - \sqrt{\alpha}\right). \tag{16}$$

Note that for Intermittent flow, the critical liquid thickness is defined similarly to the Stratified flow configuration, viz. between two slugs, the flow pattern is almost identical to the Stratified configuration.

Based on the present experimental database, good agreement has been obtained using a critical bubble radius in Eq. (11) of $r_{\mathrm{crit}} = 0.38 \times 10^{-6}$ m (best fit with respect to the experimental data).

At the present experimental conditions, the ONB value is easily reached for Stratified flow and sometimes for Stratified-Wavy flow and represents an influential parameter in Figs. 3, 4 and 8, where different heat transfer coefficients values are obtained for different heat flux levels, and also for experimental tests where the heat flux was of the same order than the ONB value (Fig. 4 at lower heat flux and Figs. 6 and 7) where the jumps in the predicted curves result from the intermittence of asymptotic and purely convective liquid heat transfer coefficients. No nucleate boiling occurs for Annular flow within the range of the heat fluxes tested.

5.3. Thermal condition for non-axisymmetric flow patterns

For Stratified and Stratified-Wavy flow patterns, the tube periphery is not completely wetted. Thus, the thermal conditions around the tube are not axisymmetric. Since the liquid coefficient is very large compared to its vapor counterpart, the heat flux from the water to the refrigerant is not uniform around the tube. A pseudo-Biot number can be defined to estimate the liquid and vapor contributions to the mean heat flux during evaporation in a specific form where the characteristic length is the distance between the top of the tube and the wetted location of the tube. As the vapor convective heat transfer coefficient is small compared to that of the liquid, it is neglected and only the liquid heat transfer coefficient is taken into account. Hence, the general form of the pseudo-Biot number becomes

$$Bi_{\mathrm{S}} = \frac{h_{\mathrm{wet}}}{\lambda_{\mathrm{w}}}\frac{1}{2}S_{\mathrm{V}} = \frac{h_{\mathrm{wet}}}{\lambda_{\mathrm{w}}}\frac{1}{2}\left(\pi - \frac{\theta_{\mathrm{wet}}}{2}\right)\frac{1}{2}\overline{D}, \tag{17}$$

where $\overline{D} = (1/2)(D_{\mathrm{in}} + D_{\mathrm{out}})$ is the mean tube diameter. The several units involved are similar to those of the classical Biot number definition. As here the characteristic length is a peripherical length, we decided to call it pseudo-Biot number to avoid confusion.

Used in the form of a parameter F_{l} varying between 0 and 1 when Bi_{S} varies from ∞ to 0 leads to

$$F_{\mathrm{l}} = \frac{1}{1 + Bi_{\mathrm{S}}}. \tag{18}$$

Very good agreement has been found for fluorocarbons and ammonia using the following empirical expression:

$$\dot{q}_{\mathrm{L}} = \frac{\dot{q}}{1 - (\theta_{\mathrm{dry}}/2\pi)\,F_{\mathrm{l}}^{p}}, \tag{19}$$

where $\dot{q}$ is the heat flux applied to the perimeter of the tube and the exponent p, based on experimental data, is defined as

$$p = -0.561x + 0.519. \tag{20}$$

5.4. Void fraction and flow pattern

As already detailed in [6] and based on the works of Zuber and Findlay [11], void fraction is dependent on flow pattern. Thus, in conjunction with the flow pattern map, the void fraction will be determined based on the local flow pattern. That is, the void fraction model of Taitel and Dukler [12] will be used in the Stratified flow region and along the Stratified to Stratified-Wavy transition boundary, the version of the Rouhani void fraction model proposed for horizontal flow in [13] will be used in the Intermittent and the Annular flow regions, and along the Stratified-Wavy to Annular/Intermittent transition boundary and an adaptation of the general drift flux void fraction solution to obtain a linear variation of void fraction in the Stratified-Wavy flow region depending on the void fraction solutions obtained at the same vapor quality will be used on the Stratified to Stratified-Wavy and on the Stratified-Wavy to Annular transition boundaries. Thus, the general drift flux solution is given as

$$\alpha = \frac{x}{\rho_{\mathrm{V}}}\left[C\left(\frac{x}{\rho_{\mathrm{V}}} + \frac{1-x}{\rho_{\mathrm{L}}}\right) + \frac{V_{\mathrm{V}}}{G}\right]^{-1}, \tag{21}$$

where the distribution factor C is given in [13] for horizontal flow as

$$C = 1 + c_0(1 - x), \tag{22}$$

where $c_0 = 0.12$ and the weighted mean drift velocity is

$$V_{\mathrm{V}} = 1.18(1-x)\left[\frac{\sigma_{\mathrm{g}}(\rho_{\mathrm{L}} - \rho_{\mathrm{V}})}{\rho_{\mathrm{L}}^2}\right]^{1/4}. \tag{23}$$

This represents the void fraction solution adopted along the Stratified-Wavy to Annular transition boundary. Applied to horizontal flow, the separated model of Taitel and Dukler [12] can be written in the following dimensional form:

$$X_{tt}^2\left[\frac{(S_L)^{1.2}}{(1-\alpha)^3}\right]-\left[\frac{(S_V+S_i)^{0.2}}{\alpha^2}\left(\frac{S_V+S_i}{\alpha}+\frac{S_i}{(1-\alpha)}\right)\right]=0. \tag{24}$$

This last void fraction solution can be obtained with Eq. (21), using Eq. (23) and adapting the distribution multiplier c_0 from Eq. (22). Fig. 18 shows the resulting variation of the distribution multiplier c_0 along the Stratified to Stratified-Wavy transition boundary for ammonia evaporated in a 14 mm ID tube at 4°C.

In the Stratified-Wavy flow region, the two values of mass velocity along the two transition boundaries (Stratified to Stratified-Wavy and Stratified-Wavy to Annular) are used to define a non-dimensional parameter as

$$\tilde{G}=\frac{G-G_{Strat}}{G_A-G_{Strat}}. \tag{25}$$

The distribution factor C in the Stratified-Wavy flow region is then obtained as

$$C_{Wavy}=C_{Strat}+\tilde{G}(C_A-C_{Strat}). \tag{26}$$

Note as a particular point that for ammonia in the previously described conditions, the distribution factor is constant for every mass velocity in the Stratified-Wavy region at a vapor quality of $x=0.25$.

The variation of the wetted angle is very difficult to predict. As the values at the Stratified to Stratified-Wavy, and at the Stratified-Wavy to Annular transitions are known (respectively $\theta_{wet,Strat}$ and 2π), the angle can be assumed to be expressed as the following dimensionless linear function:

$$\tilde{\theta}_{wet}=\frac{\theta_{wet}-\theta_{wet,Strat}}{2\pi-\theta_{wet,Strat}}. \tag{27}$$

Based on the experimental heat transfer results for ammonia at constant mass velocities of 20, 30, 40, 45 and 50 kg/(m^2 s), and at constant vapor qualities of 0.17, 0.2, 0.47, 0.5, 0.77 and 0.8, the wet angles (in radians) resulting can be fit for convenience with the following expression:

$$\tilde{\theta}_{wet}=\tilde{G}^{(38.127x^2(1-x))}. \tag{28}$$

5.5. The Stratified-Wavy region at the end of evaporation

Due to the very sensitive variations of the wetting angle and void fraction in the Stratified-Wavy flow region, it is proposed to smooth the heat transfer coefficient at the end of evaporation in two subregions. In the Dryout region, which is defined from the lowest mass velocity value of the Stratified-Wavy to Annular transition boundary until complete evaporation (refer to Fig. 19), a relative vapor quality is defined as

$$\tilde{x}=\frac{1-x}{1-x_A}, \tag{29}$$

where x_A is the value of the vapor quality corresponding to the Stratified-Wavy to Annular transition at constant mass velocity.

Calling here $h_{tp,A}$ the Annular heat transfer coefficient occurring at the onset of dryout and h_{vap} the *all vapor* heat transfer coefficient calculated with the Dittus–Boelter relation (see Eq. (7)), the two-phase flow heat transfer coefficient in this part of the Stratified-Wavy flow region is given by

$$h_{tp}=h_{tp,A}+\tilde{x}^2(h_{vap}-h_{tp,A}). \tag{30}$$

A second subregion (Fig. 20) of the Stratified-Wavy flow region is modified from the general heat transfer

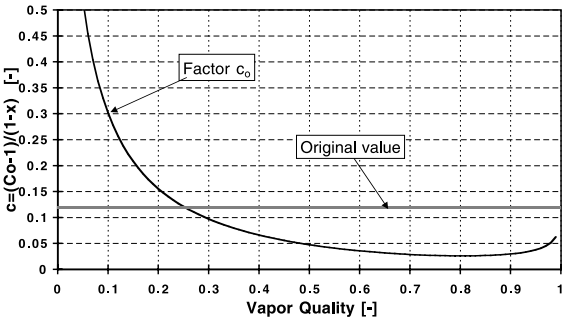

Fig. 18. Distribution factor multiplier c_0 to be applied to the equation of Rouhani to allow continuity of function along the Stratified to Stratified-Wavy transition boundary.

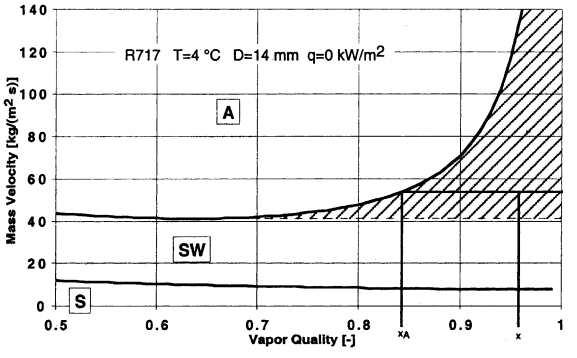

Fig. 19. Representation in the ammonia map of the onset of Dryout region after Annular flow pattern.

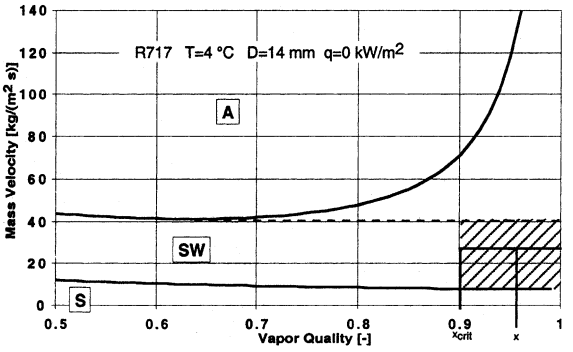

Fig. 20. Representation in the ammonia map of the Stratified-Wavy region at the end of evaporation.

procedure. Due to the need to converge to the *all vapor* heat transfer coefficient, it has been decided to linearize the evolution of the heat transfer coefficients between a Stratified-Wavy critical vapor quality value arbitrarily set at $x_{\text{crit}} = 0.9$ and the *all vapor* coefficient. The relative vapor quality has been here defined as

$$\tilde{x} = \frac{1-x}{1-x_{\text{crit}}}. \tag{31}$$

Calling here $h_{\text{tp,Wavy}}$ the Stratified-Wavy heat transfer coefficient calculated at x_{crit} and h_{vap} the *all vapor* heat transfer coefficient calculated with the Dittus–Boelter relation, the Stratified-Wavy heat transfer coefficient is given by

$$h_{\text{tp}} = h_{\text{tp,Wavy}} + \tilde{x}^2(h_{\text{vap}} - h_{\text{tp,Wavy}}). \tag{32}$$

Note that expressions (30) and (32) have been linearized with the squared value of the relative vapor quality. With this, the decrease toward the all vapor heat transfer coefficient is smooth, and conform with the experimental results. Fig. 21 summarizes the set of equations and the procedure to be followed for the implementation of the heat transfer coefficient model.

5.6. Comparison with our experimental flow boiling data

The error between the predicted and the calculated heat transfer coefficient is evaluated as

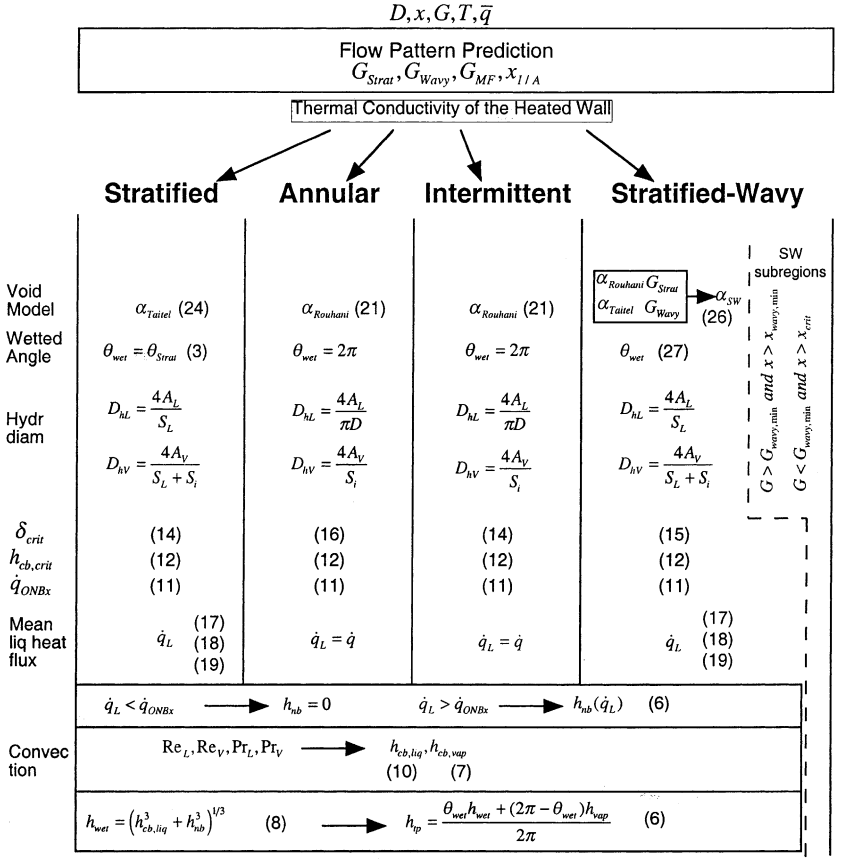

Fig. 21. General chart of the new heat transfer procedure.

$$\varepsilon_i = \frac{(h_{model} - h_{exp})}{h_{exp}}. \quad (33)$$

The standard deviation is defined as

$$\sigma = \sqrt{\frac{1}{n-1}\sum_{i=1}^{n}(\varepsilon_i - \bar{\varepsilon})^2}. \quad (34)$$

The standard deviation is certainly the most explicit expression of deviation as it provides (for $\pm\sigma$) the location of ≈65% of statistical occurrence. Twice the standard deviation value ($\pm 2\sigma$) increases the statistical occurrence to ≈95%.

Based on the analysis of all ammonia data, which represents evaporation at constant mass velocities of 10, 20, 30, 40, 45, 50, 55, 60, 80, 120 and 140 kg/(m^2 s) (640 experimental points), at constant vapor qualities of 0.17, 0.2, 0.47, 0.5, 0.77, 0.8 (173 experimental points) in a heat flux range varying from 5 to 70 kW/m^2, and evaporation at constant mass velocities of refrigerant HFC-134a at 100, 200, 300 kg/(m^2 s) in a heat flux range varying from 2 to 5 kW/m^2 (66 experimental points), covering all the four described flow patterns (Stratified, Stratified-Wavy, Intermittent and Annular), the standard deviation is 27.9% and the average deviation is −1.70%, which is a very reasonable result in two-phase flow boiling. Note that these statistical results are not really representative of the accuracy of the proposed model. It must be understood that our experimental work focused on the transitional zones where it is much more difficult to predict heat transfer rates. Thus, a large portion of the experimental points where obtained in transitional regions while only the necessary points were tested where the flow conditions were clearly established. Comparisons are made to our database in Figs. 3–14.

5.7. Comparison of the new correlation to independent data

Only a few true local heat transfer coefficient measurements are found in the literature for comparison to our heat transfer model. These are presented below.

Zürcher et al. [5] tested the model of Kattan [4] with reasonable accuracy and then included some empirical modifications to the flow boundaries to better match the experimental visualizations and the flow map. Comparison of this intermediate model was made with the ammonia flow boiling data of Chaddock and Buzzard [14]. They made tests for a carbon steel tube (13.39 mm internal diameter) at low pressures, albeit for an electrically heated test section operating at saturation temperatures of ($T = -34.4$°C, $G = 16.3$ kg/(m^2 s)), ($T = -26.1$°C, $G = 32.6$ kg/(m^2 s)), ($T = -21.8$°C, $G = 65.2$ kg/(m^2 s)) and ($T = -21.6$°C, $G = 130.5$ kg/(m^2 s)) all for a constant heat flux of $\dot{q} = 12.6$ kW/m^2.

Fig. 22 shows the flow pattern map obtained with the new model at a saturation temperature of −26.1°C. Compared to the flow map obtained at −4°C published in [6], the Stratified-Wavy to Annular transition occurs at lower mass velocities by about 20 kg/(m^2 s) based on the additional flow observations now available.

Fig. 23 shows the comparison of the original Kattan [4], the new and the experimental heat transfer coefficients obtained by Chaddock and Buzzard [14]. Even if the saturation temperature range is far below the present database, very good agreement at low mass velocity ($G = 16.3$) and at $G = 32.6$ kg/(m^2 s) is obtained.

At $G = 65.2$ kg/(m^2 s) the new model predicts Annular flow while the shape of the experimental curve does not seem to suggest this flow regime. There are not enough data points to make further comments, as the principle indication for Annular flow is the typical peak at the end of evaporation. Note also that the experimental points obtained during this work do not agree with the experimental points of Chaddock and Buzzard [14] for this mass velocity and for one of his two conflicting datasets at $G = 130.5$ kg/(m^2 s) shown in Fig. 23 for identical test conditions.

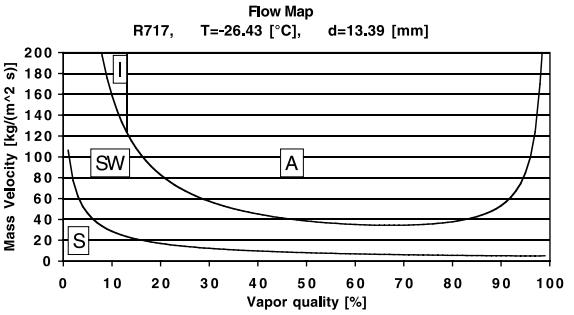

Fig. 22. Flow pattern map at −26.1°C (S = Stratified, SW = Stratified-Wavy, I = Intermittent, A = Annular).

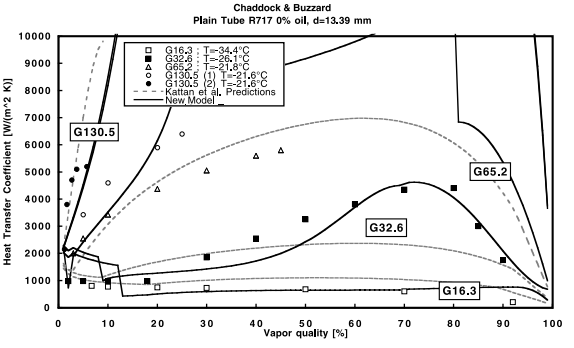

Fig. 23. Experimental points of Chaddock and Buzzard [14] at −26.1°C compared to the model of Kattan [3] and the new heat transfer model.

The new heat transfer model better predicts the results at low mass velocity than the previous numerical modification of boundaries proposed in [5].

Sandru and Chiriac [15] made experimental tests with ammonia evaporating in a horizontal tube over a wide range of mass velocities ($200 < G < 600$ kg/(m^2 s)) at very small vapor qualities ($0.2\% < x < 2\%$) in a temperature range varying from $-5°C < T < 5°C$ and a heat flux range of $7 < \dot{q} < 25$ kW/m^2. They recognized that heat transfer was mainly governed by the nucleate boiling phenomenon at this low vapor quality. Based on their experimental tests, they found a relation for nucleate pool boiling where the exponent applied on heat flux was 0.67. This is the same value adopted by Cooper [8], which is adopted in this work in Eq. (9).

6. Conclusion

An improved heat transfer model has been proposed, specific to each flow pattern, and has been compared to the experimental flow visualizations and local heat transfer coefficient measurements:

- The liquid film in the Annular flow geometry is represented with a turbulent convective heat transfer model for liquid Reynolds number values down to $Re_{D,Lw} \approx 580$.
- The Stratified flow region is mainly driven by the nucleate pool boiling phenomenon and a heat flux correction using a pseudo-Biot number proposed here to account for conduction in the tube wall. In this case, the local heat transfer model is asymptotic. As the heat transfer models of the Stratified and the Annular flow patterns are different, an onset of nucleate boiling criterion has been defined based on the definition of the pool boiling conditions and adapted to the flow condition by the use of the critical convective heat transfer coefficient occurring at the thickest location in the liquid layer of a given flow geometry.
- The Intermittent flow region has been considered to be an all wetted region where the onset of nucleate boiling has been defined at the thickest point of the Stratified liquid layer.
- The Stratified-Wavy region has been geometrically treated with the two-circle representation for the definition of the wetted angle, while the heat transfer coefficient has been calculated with the mean liquid thickness defined by a linearization of void fraction between Stratified and Annular flow.

At low mass velocity, the heat flux is a parameter involved in the heat transfer prediction in the form of the asymptotic approach. Increasing the mass velocity, the flow becomes Stratified-Wavy and rapidly increases to Annular heat transfer properties defined with a typical slope of the coefficient during evaporation and the peak at the onset of dryout at high vapor quality. The nucleate boiling contribution is reduced when the mass velocity is increased and tends to act only in the low vapor quality region. When the flow reaches the Annular flow regime, the heat transfer coefficients are modelled with the purely convective model (without nucleate boiling below the threshold for $\dot{q}_{ONB,x}$).

These experimental results confirm the proposed relation for the onset of nucleate boiling and agree well with the pseudo-Biot function needed to define the wet and dry perimeter heat fluxes applied to each phase separately in stratified types of flow.

The new heat transfer model has been compared to the experiments of Chaddock and Buzzard [14] with very good agreement to their low mass velocity heat transfer results. Sandru and Chiriac [15] obtained an empirical nucleate boiling relation with the same exponent as Cooper [8] correlation, the latter which is used in the new model.

This work has focused on the ammonia results as this database, which covers a very large number of experimental points compared to the other refrigerants tested (HFCs). Nevertheless, the HFC data have also been successfully predicted with the new model.

Acknowledgements

This work has been carried out at the Laboratory for Industrial Energy Systems (LENI) in collaboration with the Laboratory of Heat and Mass Transfer (LTCM), Swiss Federal Institute of Technology in Lausanne (EPFL). The project has been partially supported financially by the Swiss Federal Office of Energy (OFEN), which is gratefully acknowledged.

References

[1] N. Kattan, J.R. Thome, D. Favrat, Flow boiling in horizontal tubes. Part 1: development of a diabatic two-phase flow pattern map, J. Heat Transfer 120 (1998) 140–147.

[2] N. Kattan, J.R. Thome, D. Favrat, Flow boiling in horizontal tubes. Part 2: new heat transfer data for five refrigerants, J. Heat Transfer 120 (1998) 148–155.

[3] N. Kattan, J.R. Thome, D. Favrat, Flow boiling in horizontal tubes. Part 3: development of a new heat transfer model based on flow patterns, J. Heat Transfer 120 (1998) 156–165.

[4] N. Kattan, Contribution to the heat transfer analysis of substitute refrigerants in evaporator tubes with smooth or enhanced tube surfaces, Ph.D. Thesis No. 1498, Swiss Federal Institute of Technology in Lausanne, Switzerland, 1996.

[5] O. Zürcher, J.R. Thome, D. Favrat, Evaporation of ammonia in a smooth horizontal tube: heat transfer measurements and predictions, J. Heat Transfer 121 (1999) 89–101.

[6] O. Zürcher, D. Favrat, J.R. Thome, Development of a diabatic two-phase flow pattern map for horizontal flow boiling, Int. J. Heat Mass Transfer 45 (2002) 291–301.
[7] O. Zürcher, Contribution to the heat transfer analysis of natural and substitute refrigerants evaporated in a horizontal tube, Ph.D. Thesis No. 2122, Swiss Federal Institute of Technology in Lausanne, Switzerland, 2000.
[8] M.G. Cooper, Saturation nucleate boiling: a simple correlation, in: 1st U.K. National Conference on Heat Transfer, vol. 2, pp. 785–793 (I. Chem. E. Symposium Series No. 86, 1984).
[9] O. Zürcher, J.R. Thome, D. Favrat, An onset of nucleate boiling criterion for horizontal flow boiling, Int. J. Thermal Sci. 39 (9) (2000).
[10] D. Steiner, J. Taborek, Flow boiling heat transfer in vertical tubes correlated by an asymptotic model, Heat Transfer Eng. 13 (2) (1992) 43–69.
[11] N. Zuber, J.A. Findlay, Average volumetric concentration in two-phase flow systems, J. Heat Transfer 87 (1965) 453–468.
[12] Y. Taitel, A.E. Dukler, A model for predicting flow regime transitions in horizontal and near horizontal gas–liquid flow, AIChE J. 22 (1) (1976) 47–55.
[13] D. Steiner, in: VDI-Wärmeatlas (VDI Heat Atlas) (Edited by Verein Deutscher Ingenieure, VDI-Gesellschaft Verfahrenstechnik und Chemieingenieurwesen (GCV), Translator: J.W. Fullarton), Chap Hbb. Düsseldorf, 1993.
[14] J. Chaddock, G. Buzzard, Film coefficients for in-tube evaporation of ammonia and R-502 with and without small percentages of mineral oil, ASHRAE Trans. 92 (Part 1A) (1986) 20–40.
[15] E. Sandru, F. Chiriac, Heat transfer for the vaporisation of ammonia during flow through horizontal pipe systems under conditions of low vapor concentration, Int. Chem. Eng. 18 (4) (1978) 692–699.
[16] F.W. Dittus, L.M.K. Boelter, University of California Publications on Engineering (Berkeley) 2 (1930) 443.